Synthesis of Iron Oxide Nanostructures by Annealing Electrodeposited Fe-Based Films

Baoyu Zong,*,† Yihong Wu,‡ Guchang Han,† Bingjun Yang,† Ping Luo,† Li Wang,† Jinjun Qiu,† and Kebin Li†

Data Storage Institute, DSI Building, 5 Engineering Drive 1, Singapore 117608, Republic of Singapore, and Department of Electrical and Computer Engineering, National University of Singapore, Singapore 119260, Republic of Singapore

Received September 7, 2004. Revised Manuscript Received December 30, 2004

We report the self-assembly of microsized nanowalls and nano-/micropatterns of magnetic iron oxides upon the oxidation of electrodeposited Fe-based films when annealed in air at temperatures ranging from 300 to 450 °C. Scanning electron microscope studies indicate that these nanowalls have the thinnest wall of down to ∼8 nm with a length up to ∼2 μm and a height reaching ∼6 μm; the square patterns have an area of 0.06−1.0 μm^2. The generated nanowalls can be used to detect O_2 or H_2 at high temperatures via their resistance change. The simple spontaneous synthesizing procedure reported here can be applied as well to other electro-/electroless-deposited metal films to form zero-, one-, and two-dimensional metal-based nanostructures.

Introduction

Metal-based nanomaterials are currently being extensively investigated and used to develop various types of nano-devices[1−3] because of their two merits. First, they display unique properties at the nanoscale regime that are not seen in their bulk phases;[4,5] second, functional nanoscale devices can overcome fundamental and economic limitations of conventional lithography-based fabrications.[6] To date, many interesting metal-based nanomaterials and nanostructures have already been synthesized.[7−11] However, the common fabricating methods used presently are molecular beam epitaxy (MBE), laser ablation, metal−organic chemical vapor deposition (MOCVD), and electron beam evaporation. Moreover, most of the nanomaterials reported are of zero-dimensional (0D) and one-dimensional (1D) structures. It is therefore a challenge to find innovative ways to fabricate metal-based nanomaterials with two-dimensional (2D) structures at low cost and in a simple manner.

Particularly, increasing attention is being paid to ferromagnetic nanomaterials, which are widely used in catalysis, magneto-electronic devices, anticorrosion protective paints,[12,13] target drugs, cell separation, and enzyme immunoassay.[14,15] Despite the successful fabrication of iron nanoparticles[16,17] and nano-triangular-facet Fe_3O_4 films,[18] 2D magnetic nanomaterials with microsize (in length or height) structures have not been achieved so far. As compared to nanosize nanomaterials, microsize nanomaterials possess larger surface area and thus are more suitable to some applications such as catalyst beds in biomedical reactions and magnetic substrates in absorption of electromagnetic waves. Herein, we present a simple method to fabricate 2D microsize Fe_2O_3 nanowalls and square iron oxide nano-/micropatterns by annealing electrodeposited Fe-based films in air. Magnetic measurements by the vibrating sample magnetometer (VSM) displayed an increase in the coercivity (H_c) of the nanowalls and a decrease in the remnant moment (M_r) as compared to the original Fe-based films. The electrical measurement of nanowall resistance showed that the nanowalls were sensitive to O_2 and H_2 at high temperatures (above 80 °C). We have also demonstrated that square patterns could be generated by annealing thin Fe-based films in a magnetic field. A mechanism is being proposed to account for the formation of these nano-/microstructures.

* Corresponding author. Tel.: 65-6874 8411. Fax: 65-6777 1349. E-mail: zong_baoyu@dsi.a-star.edu.sg.
† Data Storage Institute.
‡ National University of Singapore.

(1) Xiao, Y.; Patolsky, F.; Katz, E.; Hainfeld, J. F.; Willner, I. *Science* **2003**, *299*, 1877.
(2) Ohno, H. *Science* **1998**, *281*, 951.
(3) Melosh, N. A.; Diana, F.; Gerardot, B.; Bdolto, A.; Petroff, P. M. *Science* **2003**, *300*, 112.
(4) Mathur, S.; Veith, M.; Sivkov, V.; Shen, H.; Huch, V.; Hartmann, V.; Gao, H. B. *Chem. Vap. Deposition* **2002**, *8*, 277.
(5) Fendler, J. H. *Nanoparticles and Nanostructured Films*; Wiley-VCH: Weinheim, 1988.
(6) Heath, J. R.; Kuekes, P. J.; Snider, G. S.; William, R. S. *Science* **1998**, *280*, 1716.
(7) Yang, B. J.; Wu, Y. H.; Zong, B. Y.; Shen, Z. X. *Nano Lett.* **2002**, *2*, 751.
(8) Goldberger, J.; He, R.; Zhang, Y. F.; Lee, S. K.; Yang, H. Q.; Choi, H. J.; Yang, P. D. *Nature* **2003**, *422*, 599.
(9) Zach, M. P.; Ng, K. H.; Penner, R. M. *Science* **2000**, *290*, 2120.
(10) Ng, H. T.; Li, J.; Smith, M. K.; Nguyen, P.; Cassell, A.; Han, J.; Meyyappan, M. *Science* **2003**, *300*, 1249 (in Brevia).
(11) Lao, J. Y.; Huang, J. Y.; Wang, D. Z.; Ren, Z. F. *Nano Lett.* **2003**, *3*, 235.
(12) Bradley, F. N. *Materials for Magnetic Functions*; Hayden: New York, 1976.
(13) Hibst, H. *J. Magn. Magn. Mater*. **1988**, *74*, 193.
(14) Ugelstad, J.; Berge, A.; Ellingsen, T.; Schmid, R.; Nilsen, T. N.; Mark, P. C.; Stenstad, P.; Hornse, E.; Olsvik, Ø. *Prog. Polym. Sci.* **1992**, *17*, 87.
(15) Liu, X. Y.; Ding, X. B.; Zheng, Z. H.; Peng, Y. X.; Chan, A. S. C.; Yip, C. W.; Long, X. P. *Polym. Int.* **2003**, *52*, 235.
(16) Choi, H. C.; Kundari, S.; Wang, D. W.; Javey, A.; Wang, Q. A.; Rolandi, M.; Dai, H. J. *Nano Lett*. **2003**, *3*, 157.
(17) Reiss, B. D.; Mao, C. B.; Solis, D. J.; Ryan, K. S.; Thomson, T.; Belcher, A. M. *Nano Lett*. **2004**, *4*, 1127.
(18) Nikiforov, M. P.; Vertegel, A. A.; Shumsky, M. G.; Switzer, J. A. *Adv. Mater*. **2000**, *12*, 18.

10.1021/cm0484697 CCC: $30.25
Published on Web 02/18/2005

Experimental Section

Iron-based films were electrodeposited on the following substrates: 99.9% pure Cu plates (111, 220), Si (100) wafers, or SiO_2 (amorphous) wafers. Before electrodeposition of the Fe-based films, seed layers such as Au (111), Cu (111), or NiFe (220) with the thickness of 35 nm were sputtered on the Si or SiO_2 wafers at room temperature to act as electrical conducting layers for the electroplating. The surface roughness (R_q) of the pure Cu plates was around 8.5 nm, while that of the seed layers was around 0.3 nm. In our studies, the Fe-based films were FeMn films containing a low atomic ratio of manganese. The $Fe_{100-x}Mn_x$ ($x = 0-32$) films were electrodeposited at 45 °C from a solution of 0.1 mol/L $FeSO_4 \cdot 7H_2O$, 0−0.5 mol/L $MnSO_4$, and 0.3 mol/L H_3BO_3. The electroplating bath was 1.2 L Paddle-Cell (Uyemura, Japan), and the DC source was pulse power (EG&G 273A) with a scanning rate of 100 mA/s.

Annealing was carried out on a hotplate (Cimrec 2, Thermolyne) in air. Temperature of the annealing ambience was controlled at 23 ± 2 °C, and humidity of the ambience was kept in the range of 70−80%. Scanning electron microscopy (SEM) images were obtained using a field-emission microscope (JSM-6340F, JEOL Asia) operated at an acceleration voltage of 15 kV. X-ray diffraction (XRD) pattern was recorded from a powder sample using Philips PW-1710 diffractometer (Cu Kα radiation, $\lambda = 1.5406$ Å) at a scanning rate of 0.02°/s in 2θ ranging from 20° to 80°. An energy dispersive spectroscopy (EDS) attached to the SEM was used to identify the ratio of Fe and Mn in the FeMn films. Magnetic measurements of the nanowalls were carried out with a VSM (Lake Shore 735, Inc.).

Results and Discussion

The generation of iron oxide nanowalls is found to be affected by various factors such as composition and thickness of the FeMn films, annealing temperature and time, substrates used, and so on. In this section, first, we address the effects of these factors; second, we discuss the mechanisms associated with the generation of the nanowalls and square patterns in detail; and, finally, characterization and application of the nanowalls are illustrated.

A. Effects of Influential Factors. *a. Effect of Film Composition.* The composition of the FeMn film is determined by the electrodepositing current density (ECD) in a Mn-contained solution. When the ECD was increased from 5 to 70 mA/cm^2, the Mn:Fe atomic ratio in the deposited films increased from 1:99 to 32:68. The R_q of the deposited films also increased from 5 to 150 nm. Through our experimental results, we found that the compositions of the deposited films were similar even with the use of different substrates when the ECD was kept constant. Figure 1a_{1-3} shows the SEM images of $Fe_{81}Mn_{19}$, $Fe_{94}Mn_6$, and $Fe_{98}Mn_2$ films annealed in air at 400 °C for 10 h. These 1.0 μm films were electrodeposited from ECD of 30, 20, and 6 mA/cm^2, respectively. It can be seen that as the ECD decreases from 30 to 20 mA/cm^2, the surfaces of the annealed films change from a rough surface (Figure 1a_1) to a nanowall structure (Figure 1a_2). When the ECD is further reduced to 6 mA/cm^2, the nanowall density becomes very low (Figure 1a_3). After a series of ECD tests, we concluded that only the FeMn films deposited with ECD ranging from 8 to 25 mA/cm^2 could transform to uniform (even distribution in an area of bigger than 10 μm^2) nanowalls. The chemical formulas of these films were $Fe_{98-92}Mn_{2-8}$, and the R_q of the films was less than 30 nm. From XRD measurements, the $Fe_{98-92}Mn_{2-8}$ films were identified as a mixture of face-centered cubic and body-centered cubic crystals.

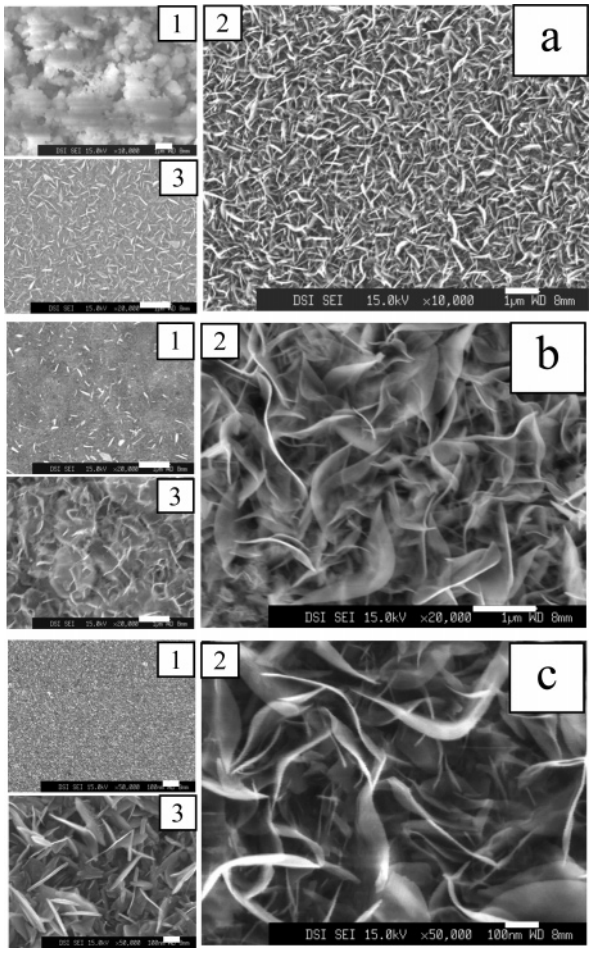

Figure 1. SEM images of the annealed FeMn films: (a_{1-3}), annealed $Fe_{81}Mn_{19}$, $Fe_{94}Mn_6$, and $Fe_{98}Mn_2$ films, respectively, on Au/SiO_2 substrates; (b_{1-3}), at 250, 400, and 500 °C, respectively, annealed $Fe_{96}Mn_4$ films on the NiFe/Si substrates; (c_{1-3}), annealed 0.3, 1.0, and 2.2 μm $Fe_{94}Mn_6$ films, respectively, on the Cu/SiO_2 substrates. The scale bar of (a) and (b) is 1 μm, while that of (c) is 100 nm.

b. Effect of Annealing Temperature. To investigate the influence of annealing temperature on the formation of iron oxide nanowalls, FeMn films with the same thickness and substrates were heated on the hotplate for 10 h at various temperatures ranging from 100 to 550 °C. The temperature of the sample surface, as measured with an infrared thermometer (Oakton), was always about 3 °C lower than that of the hotplate surface. Figure 1b_{1-3} shows SEM images of three 1.0 μm $Fe_{96}Mn_4$ films heated for 10 h at 250, 400, and 500 °C, respectively. Our investigating results indicated that uniform iron oxide nanowalls were only formed in the range of 300−450 °C (Figure 1b_2 shows a typical annealing result at 400 °C). Beyond this range, the density of the nanowalls decreased and the surfaces of the films roughened (see Figure 1b_1 and 1b_3, respectively).

c. Effect of Film Thickness. Figure 1c_{1-3} shows SEM images of annealed $Fe_{94}Mn_6$ films with different electrodeposited thickness. The annealing was performed at 400 °C for 10 h. The 0.3 μm film failed to produce nanowalls, while

the 2.2 μm film converted to small size nanowalls with only 0.5 μm of length. Their postannealing surfaces are shown relatively in Figure $1c_1$ and $1c_3$. From the observation of more detailed examinations on the electrodeposited film thickness dependence of surface morphology, we concluded that the thickness of the FeMn films should fall in the range of 0.4−1.5 μm to generate microsize nanowalls (Figure $1c_2$).

d. Effect of Substrate. From the Figure 1 images, we analyzed the effect of the substrates as well. The films of Figure 1a, b, and c were deposited on Au/SiO_2, NiFe/Si, and Cu/SiO_2 substrates, respectively. The $Fe_{94}Mn_6$ films of Figure $1a_2$, $1b_2$, and $1c_2$ were annealed at 400 °C for 10 h. Their images corresponding to the magnification of 10 000×, 20 000×, and 50 000× show similar nanowalls of iron oxide generated on different seed layers and wafers. At the beginning of the investigation of the substrate effect, we have assumed that the nanowall shape was determined by the surface morphology of the annealed seed layers. The 35 nm Au (111, fcc), Cu (111, fcc), and NiFe (220, fcc) seed layers were sputtered onto the Si wafers, and then onto the SiO_2 wafers. The two groups of substrates were both heated at 400 °C for 10 h on the hotplate. The color of all seed layers changed after annealing. The SEM studies showed that some metals of the seed layers (including gold) had been oxidized and evaporated, which led to pinholes and rough surfaces for both group substrates. The R_q of the annealed seed layer surfaces increased to the range of 3 (Au)−13 nm (Cu) by AFM measuring. Although there are some differences in the R_q among the annealed seed layers, the images of Figure $1a_2$, $1b_2$, and $1c_2$ indicate that the choices of seed layers and wafers are not critical factors in generating iron oxide nanowalls. However, it is noted that the formation of nanowalls on Cu or Au seed layers is faster than that on NiFe layer due to better heat conductivity of Cu and Au. When FeMn films were electrodeposited on pure copper plates, the annealed FeMn films broke into separated nanowall areas and some copper nanowires grew out from the breaks. The shape of the CuO nanowires obtained is similar to that of the nanowires synthesized from copper substrates.[19]

e. Effect of Annealing Duration. Figure 2a,b shows SEM images of 1.0 μm $Fe_{94}Mn_6$ films which were annealed at 400 °C for 10 and 25 h, respectively. It is obvious that the nanowall wall thickness decreases as annealing time is increased from 10 to 25 h. Under the image of high magnification up to 100 000×, the thinnest wall of the nanowalls in Figure 2a and Figure 2b samples is found to be ∼14 and ∼8 nm, respectively. Thinner walls can be achieved with longer annealing time. The nanowall cross-section view (Figure 2c) of sample 2b shows that the height of the nanowalls is around ∼6 μm.

f. Annealing of Pure Fe Films. To compare with the annealing results of the FeMn films, pure Fe films deposited from the $MnSO_4$-free solution were also annealed. Figure 2d shows the annealed image of 1 μm pure iron film. As compared to 1 μm FeMn films (Figure 2a) annealed under the same conditions (such as annealing temperature and annealing time), pure Fe film was unable to form similar uniform nanowalls after annealing.

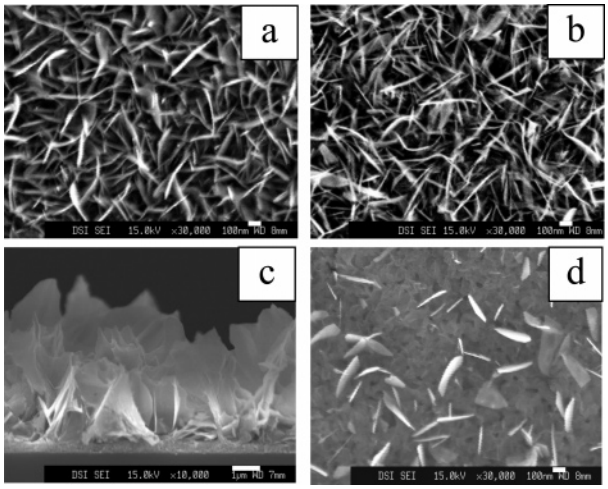

Figure 2. SEM images of (a,b) the 1.0 μm $Fe_{94}Mn_6$ films (on the Au/SiO_2 substrates) annealed for 10 and 25 h, respectively, (c) the cross-section view of sample b, and (d) the 1.0 μm pure Fe film (on the Au/SiO_2 substrate) annealed at 400 °C for 10 h. The scale bar of (a), (b), and (d) is 100 nm, while that of (c) is 1 μm.

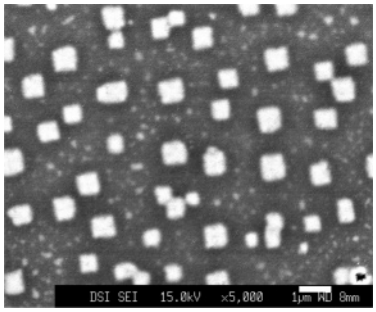

Figure 3. SEM image of 200 nm $Fe_{96}Mn_4$ film (on the Cu/Si substrate) annealed at 400 °C for 3 h. The scale bar is 1 μm.

g. Annealing of Thin FeMn Films. In the following, we investigated the effect of annealing thin (<300 nm) FeMn films. The thin films were deposited on Au/Si or Cu/Si substrates and were annealed in air under a ∼200 Oe magnetic field applied normal to the sample surfaces. Figure 3 shows that 200 nm thin $Fe_{96}Mn_4$ film is transformed into 0.1−1.0 μm^2 square patterns instead of nanowalls after heating at 400 °C for 3 h. Further investigation showed that the pattern size was decided by the annealing time. Shorter annealing time led to smaller patterns. However, no obvious square pattern was observed under the SEM image if annealing time was less than 30 min. The smallest pattern observed had dimension of 60 nm^2. On the basis of EDS analysis (see Appendix 1), the square patterns were identified as iron oxide. It is noted that a few atoms forming a 2D in-plane magnetized dot might provide a stable elementary bit for nanorecording as suggested by Stamn et al.[20]

B. Growth Mechanisms. Now we focus on the growing mechanism of the iron oxide 2D patterns and nanowalls. Based on the SEM observations, the growth of the square nano-/micropatterns may be dominated by the vapor−liquid−solid (VLS)[21,22] process, which terminates in particles by a

(19) Jiang, X. H.; Herricks, T.; Xia, Y. N. *Nano Lett.* **2002**, *2*, 12.

(20) Stamm, C.; Mrty, F.; Vaterlaus, A.; Weich, V.; Egger, S.; Maier, U.; Ramsperger, U.; Fuhrmann, H.; Pescia, D. *Science* **1998**, *282*, 449.

(21) Morales, A. M.; Lieber, C. M. *Science* **1998**, *279*, 208.

catalytic-assisted technique. As thin (<300 nm) FeMn films are annealed, vapor of the metal oxide generated from the oxidizing seed layer becomes the catalyst that leads to the termination of the iron oxide vapor at particles. Some of these iron oxide particles grow along the direction of the Si ⟨100⟩ axis and aggregate together under the effect of the magnetic field. As a result, the square patterns are formed. In our studies, we found that the square patterns were made of small nanoparticles, which could be seen under high magnification (>30 000×), and these patterns were only formed on Au/Si or Cu/Si substrate. Thin FeMn films on SiO_2 or NiFe/Si substrate could not produce these square patterns. It is probably due to the SiO_2 amorphous surface and the absence of effective catalyst produced from the NiFe seed layer.

However, SEM observation of 0.4−1.5 μm Fe films shows that the growth of nanowalls is likely to be governed by the vapor solid (VS)[23,24] process. While annealing, heat is transported from the hotplate to the iron film through the substrate. The iron oxide vapor, which evaporates from the starting oxides close to the substrate (at the higher temperature zone), directly deposits on the film surface (at a lower temperature region) and grows into nanowalls. The VS process dictates that the seed layer is not critical for the nanowall generation. In terms of thermal properties,[25] Mn is easier to oxidize and evaporate in comparison to Fe at the same temperature. After evaporation of the Mn oxide, the pinholes produced in the iron film during annealing enhance the formation of the nanowalls because they enable the starting iron oxides to evaporate easily onto the film surface. Therefore, iron films containing several percent of Mn can generate more uniform nanowalls in comparison to pure iron films. Figure 1a_2, 1b_2, 1c_2, and 2d verifies the suggested VS process. Yet a high ratio of Mn (Mn:Fe > 10:90) produces too much Mn oxide vapor, which makes the iron oxide vapor terminate at rough particles (shown in Figure 1a_1). As the starting iron oxide has difficulty in penetrating through the thick FeMn films, thus the growth of the nanowalls is slow and only some nanosize nanowalls (Figure 1c_3) were formed when the FeMn film thickness is larger than 1.5 μm.

When iron films were oxidized in air, Fe_2O_3 is suggested to be readily generated through the oxidation of FeO; FeO serves as a precursor to Fe_2O_3. Fe_3O_4 is a mixture of FeO and Fe_2O_3. The reactions involved in the entire synthesis can be summarized as the following:

$$2Fe + O_2 \rightarrow 2FeO \quad (1)$$

$$6FeO + O_2 \rightarrow 2Fe_3O_4 \quad (2)$$

$$4Fe3O_4 + O_2 \rightarrow 6Fe_2O_3 \quad (3)$$

The first reaction functions as the rate-determining step for the formation of Fe_2O_3. The slow rate for the formation of FeO ensures a relatively low pressure for this material in the reaction air zone close to the film surface and thus a continuous growth mode for the iron oxide nanowalls. On the basis of this argument, the nanowall generated from FeMn film should be Fe_2O_3. This speculation was confirmed by our XRD measurements, which showed that, except for the crystals of Fe and Fe_2O_3, no FeO and Fe_3O_4 crystals were detected.

As the Fe_2O_3 generation from FeO is determined by the Gibbs free energy (ΔG) and entropy (ΔS) of the reactions that are greatly affected by the annealing temperature, the changes of ΔG and ΔS in the reaction of $4FeO + O_2 \rightarrow 2Fe_2O_3$ (reaction 2 + 3) are similar to those in the reaction of $2Cu_2O + O_2 \rightarrow 4CuO$; therefore, the influence of the temperature on the annealing of iron films in air is consistent with that of Cu plate stated by Jiang et al.:[19] when the annealing temperatures are too high (theoretical 985 °C for the reaction of FeO → Fe_2O_3 and 964 °C for $Cu_2O \rightarrow CuO$), ΔG values of both reactions become positive, while ΔS values of both reactions become negative. This leads to the termination of formation of Fe_2O_3 or CuO. In the present study, the highest temperature for Fe_2O_3 nanowall formation decreased to ∼500 °C due to the catalyst existence of Mn oxide vapor; when the annealing temperatures are too low (250 °C for the reaction of FeO → Fe_2O_3 and 400 °C for $Cu_2O \rightarrow CuO$), the low vapor pressure of Fe_2O_3 or CuO is insufficient to form nanowalls or nanowires. The reason Fe generates nanowalls while Cu produces nanowires after annealing is so far not clear to us, and this issue deserves further explorations.

In the long duration annealing of the FeMn films, two stages may be proposed. At the initial stage of annealing, the iron films are totally converted to Fe_2O_3 nanowalls by the deep oxidization. In the second stage, the iron oxide is partially evaporated, and hence the thickness of the nanowalls decreases. Figure 2a,b verifies the suggestion.

C. Characterization of Nanowalls. Besides detailed annealing studies, the nanowalls were characterized by means of other measurements. The XRD pattern in Figure 4a shows that the nanowalls generated from the $Fe_{96}Mn_4$ film are Fe_2O_3 (410). The uniform nanowalls shown in Figure 1a_2, 1b_2, and so on were also confirmed as Fe_2O_3 with XRD results. For magnetic measurement, magnetic field was applied parallel to the surfaces of the sample substrates. Figure 4b shows that the magnetic properties of the Fe_2O_3 nanowalls are different from those of the $Fe_{96}Mn_4$ films before annealing. After annealing for 25 h, the M_r value decreased from 0.042 to 0.022 emu, and the H_c value increased from 48 to 115 Oe. When the annealing time was longer than 10 h, the XRD peaks and the properties of the annealing film became constant, which indicated that the FeMn film was fully converted into iron oxides. Based on the XRD results and magnetic properties, the Fe_2O_3 of the nanowalls should be in the single crystal γ-Fe_2O_3 phase; the proposed initial annealing stage of the FeMn film is about 10 h.

To measure the electrical properties of the Fe_2O_3 nanowalls, two gold electrodes with a gap of 1 mm were deposited on the nanowalls by evaporation. The nanowall resistance in H_2 and O_2 was measured at the temperatures of

(22) Wu, Y. Y.; Yang, P. D. *J. Am. Chem. Soc.* **2001**, *123*, 3165.
(23) Brenner, S. S.; Sears, G. W. *Acta Metall.* **1956**, *4*, 268.
(24) Shi, W. S.; Zheng, Y. F.; Wang, N.; Lee, C. S.; Lee, S. T. *Chem. Phys. Lett.* **2001**, *345*, 377.
(25) Weast, R. I., Ed. *CRC Handbook of Chemistry and Physics*, 67th ed.; CRC Press: Boca Raton, FL, 1979.

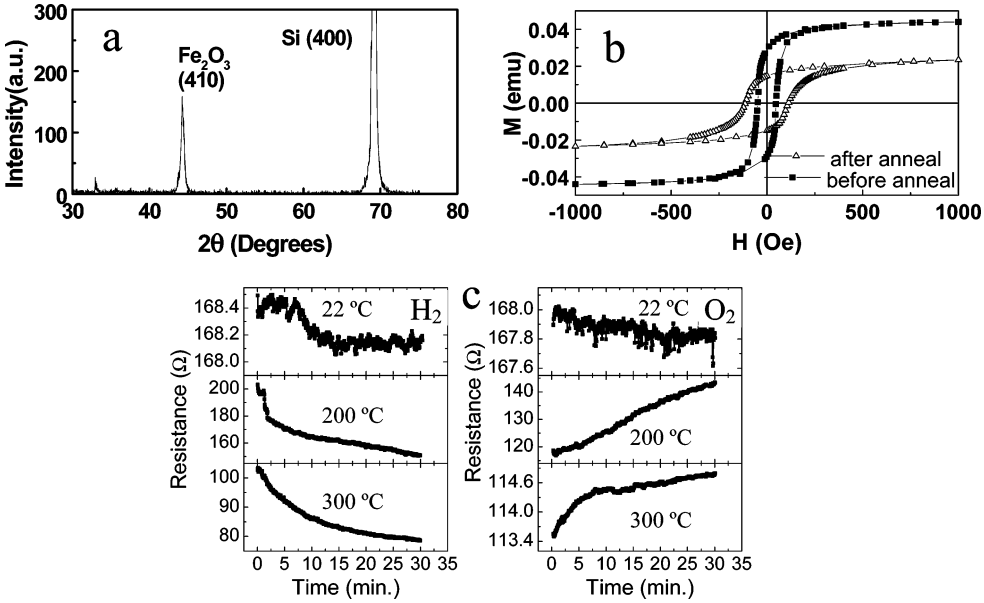

Figure 4. The properties of 1 μm $Fe_{94}Mn_6$ film (6×9 mm^2), which was deposited on the Au/SiO_2 substrate and annealed at 400 °C for 25 h: (a) the $\theta\angle\theta$ XRD result of the iron oxide nanowalls, (b) the $M-H$ loops of the film, ■ before annealing, △ after annealing, and (c) the time dependences of the nanowall resistance at different temperatures in the H_2 (left) and the O_2 (right) ambiences.

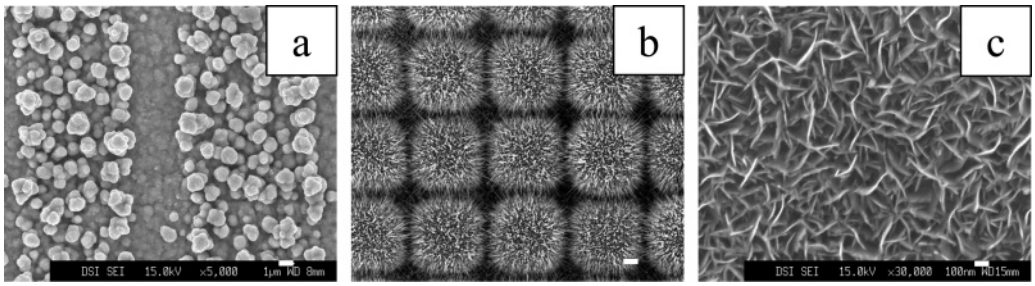

Figure 5. SEM images of the 1.0 μm electrodeposited metal films annealed at 420 °C for 8 h: (a) 0D NiO particles (diameter 80−1500 nm) from Ni film on the pattern Cu/Si substrate; (b) 1D CuO nanowires (diameter 5−180 nm, maximum length 5 μm) from Cu films on the pattern Au/Si substrate; (c) 2D Co_3O_4 nanowalls (thickness about 8 nm, height and width 0.5−2.0 μm) from Co films on the Cu/Si substrate. The scale bar of (a) and (b) is 1 μm, while that of (c) is 100 nm.

22−400 °C. Throughout the measurement, the nanowalls were immersed in a chamber with a fixed 2 Torr of H_2 or O_2. It can be seen from Figure 4c that the resistance of the nanowalls varies in large ranges (>20 Ω except in O_2 at 300 °C) at high temperatures but in narrow ranges (<2 Ω) at room temperature. When the nanowalls between the two electrodes were removed, the resistances were infinite in both gas tests. For comparison with the nanowalls, we also tested 1 μm $Fe_{96}Mn_4$ films. We found that the resistance of the $Fe_{96}Mn_4$ films in both H_2 and O_2 did not change much. For example, at 300 °C, the resistance in the H_2 environment was constant at 1.5−1.8 Ω, while the resistance in O_2 rose slightly from 1.5 to 2.5 Ω. These results and more tests indicate that Fe_2O_3 walls are sensitive to high temperatures (above 80 °C), especially around 200 °C. The change of nanowall resistance with the temperature and time is suggested as a result of Fe_2O_3 reduction and gas penetration. Under H_2 environment, the resistance of the nanowalls decreased. This is because the Fe_2O_3 is reduced to Fe, and the resistivity of Fe_2O_3 is much higher than that of Fe. At room temperature, the reduction of Fe_2O_3 by H_2 is weak, which results in small variance of the resistance; at high temperatures, more Fe_2O_3 is reduced, which leads to a huge decrease in the resistance. On the other hand, increasing the test duration results in the increased reduction of Fe_2O_3. The diffusion of the hydrogen into the nanowall crystal enhances the reduction of the Fe_2O_3. This reduction was confirmed by the repeated testing results (in which a nanowall sample was repeatedly used to measure the resistance), which showed the resistances decreasing even as the temperature was kept constant for the tests. On the contrary, the nanowall resistance with test duration increases in O_2 environment. It is probable due to the oxygen penetrating into the crystal of the thin nanowalls. With more oxygen diffusing into the crystal at a long test duration, the resistance of the nanowalls increased. Due to the fact that, at higher temperatures, the density of the O_2 in the chamber decreases at fixed pressure, there will be fewer oxygen atoms diffusing into the nanowalls at higher temperatures. Therefore, the resistance change at 300 °C is much smaller than that at 200 °C. As compared to the H_2 environment, the change of the resistance in the O_2 environment was smaller in each repeating test at the same temperature. It is because the effect of the oxygen diffusion on the resistance change is weaker than the effect of the H_2 reduction. Based on the property of the different resistance change in O_2 and H_2, the Fe_2O_3 nanowalls can be used to detect O_2 or H_2 at high temperatures (above 80 °C).

Table 1. EDS Results of the Element Component for the 200 nm Thin $Fe_{96}Mn_4$ Film (on the Cu/Si Substrate) Annealed 3 h at 400 °C

element	app concentration	intensity corrn	wt %	wt % σ	at %
O K	0.98	1.3881	0.70	0.06	45.76
Si K	0.73	0.9095	0.80	0.04	29.51
Fe K	0.65	0.8989	0.72	0.12	13.37
Cu L	0.31	0.4503	0.69	0.08	11.36
totals			2.91		

Conclusions

In summary, we have demonstrated a simple and convenient process for the synthesis of microsized Fe_2O_3 nanowalls and square nano-/micropatterns by annealing electrodeposited iron-based films in air. The nanowalls were sensitive to O_2 and H_2 at high temperatures. This process can also be used for other electro-/electroless-deposited metal and alloy films. We have applied this method to Ni, Cu, Co, and Zn films. Uniform 0D NiO nanoparticles, 1D CuO and ZnO nanowires, and 2D Co_3O_4 and ZnO nanowalls (see Appendix 2) have been successfully synthesized. The annealing procedure, when combined with other reaction processes,[26,27] may be capable of synthesizing more 0−2D nanomaterials.

Acknowledgment. We thank Mr. J. F. Chong for XRD measurements.

Appendix 1

The EDS data, which are the original measuring results, are listed in Table 1. The data indicate that the square patterns from the 200 nm thin $Fe_{96}Mn_4$ film (on the Cu/Si substrate) annealed 3 h at 400 °C are iron oxide and there is no Mn element detected because Mn, with a low atom ratio to Fe in the $Fe_{96}Mn_4$ films, is more easily evaporated than Fe.

Appendix 2

Following the same annealing procedure to synthesizing Fe_2O_3 nanowalls, 0D NiO particles, 1D CuO nanowires, and 2D Co_3O_4 nanowalls have been successfully created from the relevant electrodeposited films, as shown in Figure 5.

CM0484697

(26) Wang, S. H.; Yang, S. H. *Chem. Mater.* **2001**, *13*, 4794.
(27) Rodriguez, J. A.; Hanson, J. C.; Kin, J. Y.; Frenkel, A. I. *J. Am. Chem. Soc.* **2002**, *124*, 346.